Electronic Supplementary Material (ESI) for ChemComm.

Supporting information

Covalent organic polymer as an efficient chemosensor for highly selective H_2S detection through proton conduction

Table of contents

Materials and Methods

Section 1. Materials

6-Hydrazinonicotinic hydrazide hydrate, benzene-1,3,5-tricarboxaldehyde, acetic acid, dimethyl sulfoxide (DMSO), and all other solvents were purchased from Sigma Aldrich and Merck.

Section 2. Synthetic Procedure of COP

6-Hydrazinonicotinic hydrazide hydrate and benzene-1,3,5-tricarboxaldehyde in ethanol and 6M acetic acid solution were refluxed in 100 mL round bottom flask for 48 h at 90 °C. After that the reaction mixture was filtered and washed with methanol, acetone, dichloromethane, dimethyl sulfoxide and water. The reddish brown solid residue was dried over 80 °C for 24 h. The reddish brown solid **COP** powder was characterized by ^{13}C solid state NMR and FT-IR spectroscopy.

Section 3. Material Characterization

Solid state ^{13}C NMR spectrum was recorded using 400 MHz solid state NMR spectrometer (JEOL, model: ECX400; proton frequency: 400 MHz). Powder XRD was done on Rigaku SmartLab, Automated Multipurpose X-ray Diffractometer. Thermogravimetric analysis (TGA) was analyzed using Mettler Toledo Thermal Analyzer with heating rate of 10 °C/min. BET surface area was analyzed on Quantachrome, Autosorb iQ2. FT-IR spectra of the **COP** were recorded using Bruker, Tensor-27 FT-IR spectrophotometer. High resolution transmission electron (HRTEM) microscopy analysis was performed using Field Emission Gun-Transmission Electron Microscope 200 kV (model: Tecnai G2, F30). The field-emission scanning electron microscopy (FESEM) measurements were performed using a field-emission scanning electron microscope (Model: Supra 55 Zeiss). For FESEM measurements, the dried samples were coated with gold for subsequent imaging experiments. Atomic force microscopy (AFM) images were taken by drop-casting the samples on mica substrates *via* tapping mode at a scan frequency of 0.65-1.0 Hz and analyzed the data using SmartScan software (model park NX10).

Section 4. Gas Sensor Fabrication and Sensing Measurements

A Corning glass slide with the dimension of 3 × 3 × 0.5 mm was used for the sensor substrate. Two interdigitated Pt electrodes on the top of glass substrate were used to fabricate the sensor. Each Pt electrode consists of 5 fingers (250 × 25 × 1 μm), and the distance between two fingers was 25 μm. The **COP** powder (10 mg) in 3 mL ethanol in a 10 mL beaker was stirred and sonicated for 30 min. After that dispersed solution of the **COP** was directly drop-casted on the interdigitated electrodes coated glass substrate and dried it for the overnight at 120 °C.

The gas sensing experiment was carried out by the dynamic flow-through measurement technique (Scheme 1). The sensor resistance was monitored by Keithley-2612A source meter interfaced with PC at a direct-current (DC) voltage of 2 V. Optimal concentration of H_2S in the chamber was gained by flowing a certain amount (sccm) of synthetic air to a mixing chamber where certain amount (sccm) of test gas (H_2S) was flown. The flow rates of the respective gases were controlled by a separate mass

flow controller, MFC (model: Alicat®, MC 1slpm, USA). The temperature of the system was controlled by a PID temperature controller (with an accuracy of ±1 °C). Efficiency of the sensor corresponds to the response% is given by:

$$\text{Response (\%)} = \frac{R_g - R_a}{R_a} \times 100$$

Where R_g and R_a are the resistance of the sensor in presence of sensing gas and air.

Section S5. FT-IR stretching frequencies of benzene-1,3,5-tricarboxaldehyde and 6-hydrazinonicotinic hydrazide

FT-IR spectrum of benzene-1,3,5-tricarboxaldehyde shows a peak at 1706 cm^{-1} due to the presence of -C=O stretching mode of -CHO groups. This peak is disappeared in **COP** spectrum due to the formation of Schiff base imine. The disappearance of FT-IR peak at 1706 cm^{-1} in **COP** suggests the formation of Schiff base polymer.

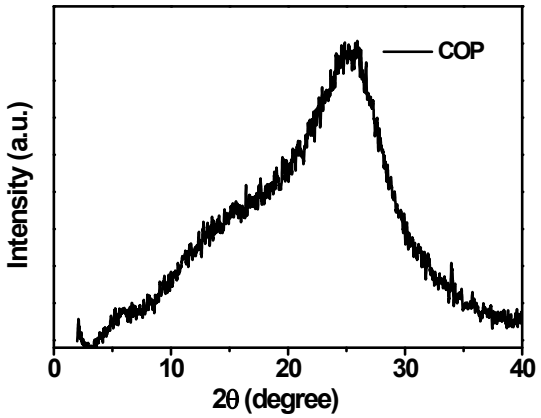

Figure S1. Wide-angle powder XRD of the **COP**.

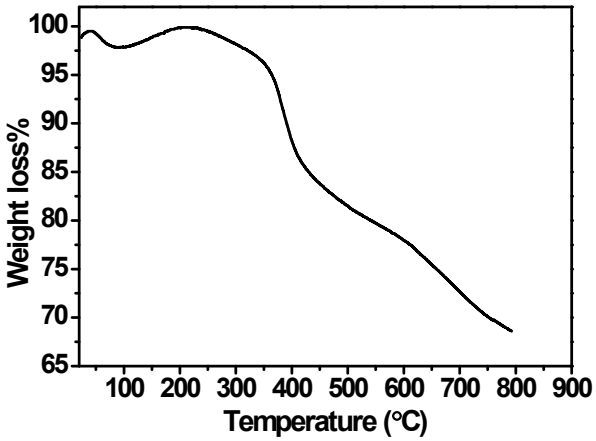

Figure S2.Thermogravimetric analysis of the **COP**.

Discussion: There is a slight increase of the mass within the temperature of 100-200 ºC. The slight increment of mass of sample within the temperature ranges is due to the buoyancy effect in TGA equipment. We impend an object in a fluid, the fluid tends to force the object upwards. Before TGA analysis, we put our sample in the analyzer chamber. The fluid (N_2) tends to force the sample upwards. Now when the analysis begins, the density of the fluid is slightly decreased with increasing the temperature and consequently the hanged sample goes down. Then we recorded these changes as mass increment but they are produced by a small change in the density of the surrounding fluid. This effect becomes less at higher temperature or heating rates.[1-3]

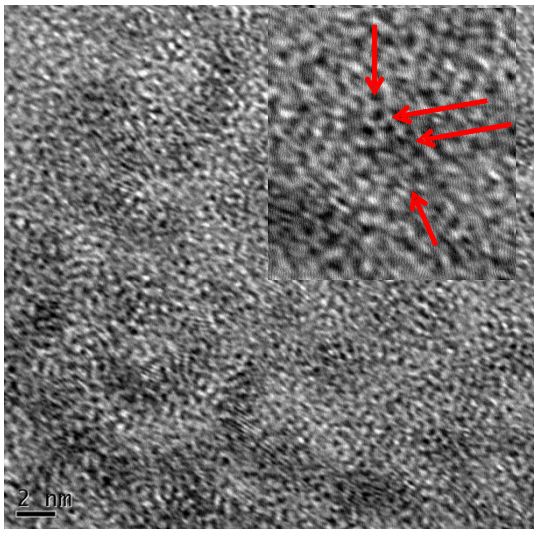

Figure S3. HRTEM image of the **COP** showing porous texture of the **COP**.

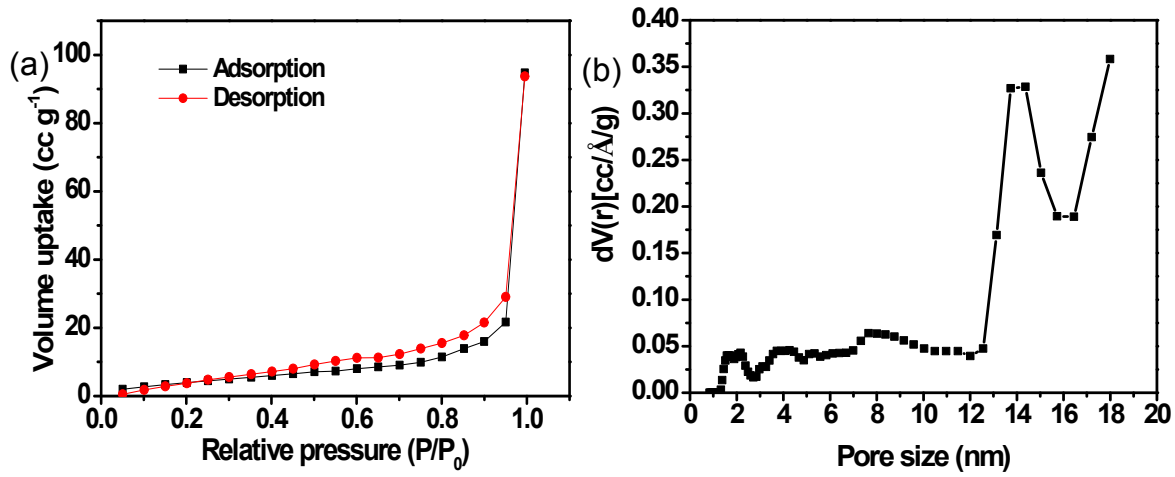

Figure S4. BET surface area analysis by N_2 adsorption and pore size distribution of the **COP** by using the NLDFT methods.

Table S1. Summary of BET surface area analysis of the **COP**

Material	N_2 uptake (cc g^{-1})	Langmuir surface area (m^2 g^{-1})	Pore size (nm)	Pore volume (cc g^{-1})
COP	94.74	452	17.5	0.29

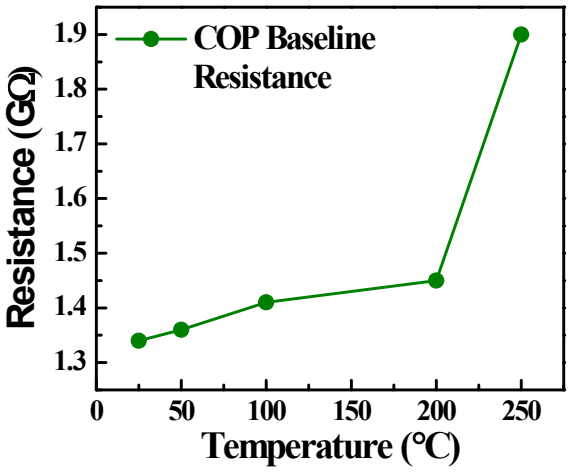

Figure S5. Resistance of the **COP** based sensor vs operating temperature.

Table S2. Comparison table of H_2S sensing of the **COP** with other reported nanomaterials based chemiresistive sensor

S. No	Material	Response time	Maximum response%	Temp. (°C)	Ref.
1	Zn-doped-Fe_2O_3 nanowire	16 s	23.5 (5 ppm H_2S)	175	20 c
2	Fe_2O_3@CNT-3.0	30 s	~ 9 (100 ppm H_2S)	25 °C	20 d
4	$MoSe_2$	15 s	19-20 (5.45 ppm)	200 °C	20 e
5	Au-nanowire	15 min	30-40 (0.5 ppm)	25 °C	20 f
6	SnO_2/rGO nanocomposites	2-13 s	60-70 (100 ppm)	22 °C	20 g
7	**COP**	9 s	50-60 (200 ppm), 30-40 (50 ppm)	25 °C	This work

Section 6. Proposed H_2S sensing mechanism of **COP** through proton conduction phenomenon

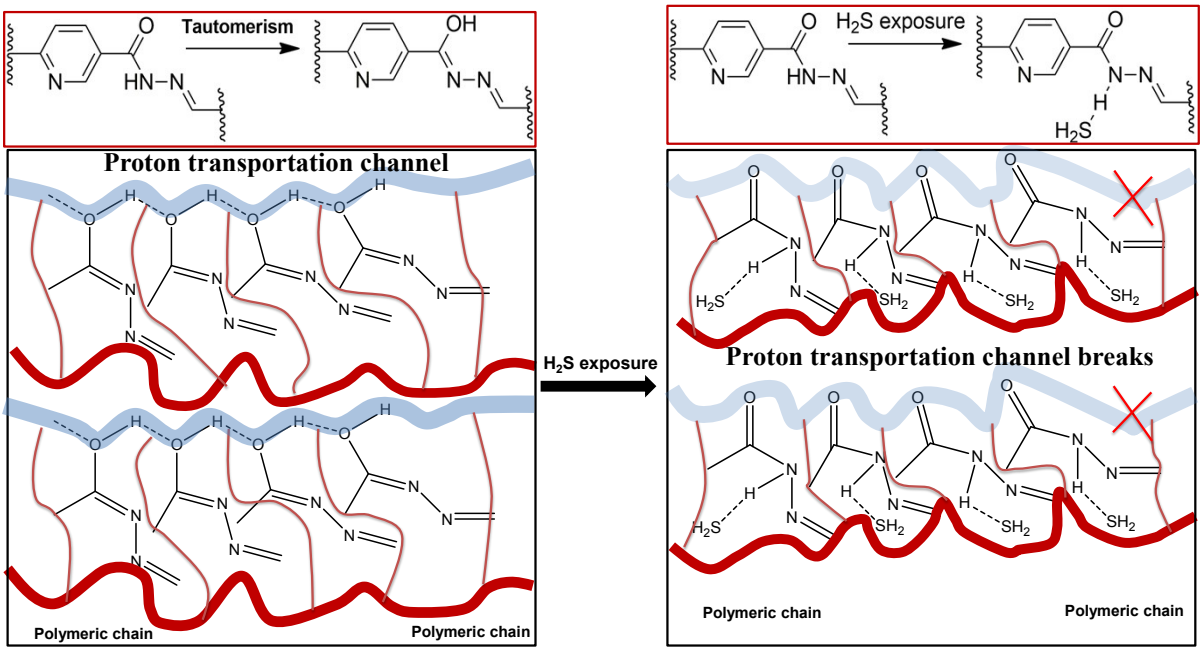

Scheme S1. Proposed schematic representation of H_2S sensing of **COP** through proton conduction.

Here, we proposed chemiresistive gas sensing mechanism. The **COP** creates a proton transportation channel inside the polymeric chain due to proton transfer of the enol form of hydrazide groups (-C(-OH)N-N=).[4-7] After H_2S exposure, the proton transportation channel gradually collapses due to $H_2S\cdots$H-N-(C=O) interaction.[8] Obviously, in H_2S environment the stability or percentage of enol form becomes lower due to $H_2S\cdots$H-N-(C=O) interaction. As a result, the electrical resistance of **COP** increases in presence of H_2S and we get very fast response. We observed that the response time becomes less at higher ppm of H_2S and very fast increment of electrical resistance of the system.

Here, the gas sensing mechanism does not occur only through the acid base interaction, however it also depends on the surface area of adsorbant, pore size and rate of adsorption-desorption of the analytes (here gases).

However, we tried to establish this through the theoretical insight. Density functional theory (DFT) calculations have been performed using Gaussian 09 software. First, the geometry of the truncated **COP** (named COPT**)** with C(=O)NH-N=) functionality has been optimized as C(=O)NH-N=) groups which mainly involves the sensing mechanism. Then the calculation is performed with a truncated version of **COP**, one molecule of H_2S and CO_2. The energy of COPT before the interaction with H_2S and CO_2 is -737.293 Hartree. Now the total energy of the H_2S-COPT system is lowered (became more negative) value of -1134.694 Hartree than CO_2-COPT with energy of -924.809 Hartree. From the energy calculation study, we conclude that H_2S-COPT system is more energetically stable and favourable system than CO_2-COPT system. So H_2S should have more tendencies to interact with **COP** than CO_2.

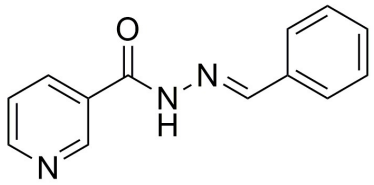

COPT

Here, we have calculated the pK_a value of **COPT** (AH) using DFT calculation.[4] The pK_a value of **COPT** is calculated as high as 51.072. Now **COPT** behaves almost like an aliphatic hydrocarbons compound due to very high pK_a value. So acid-base type of interaction with external analytes (acidic gases) is insignificant in here.

Calculation of pK_a value:

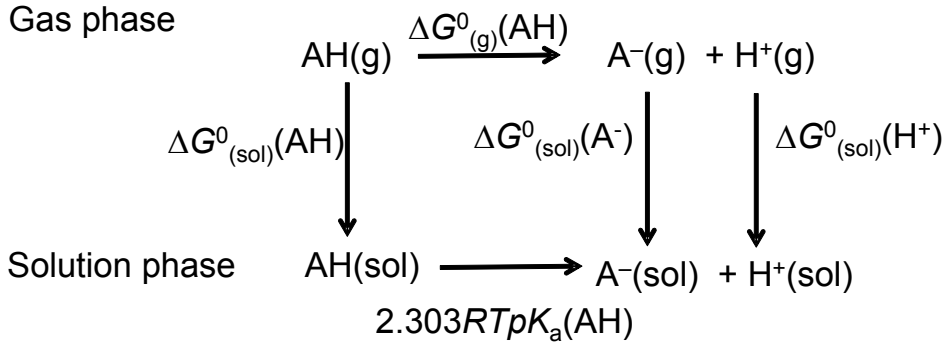

Thermodynamic cycled used for the calculation of pK_a values.

$\Delta G^0_{(g)}(AH) = \Delta G^0_{(sol)}(A^-) + \Delta G^0_{(sol)}(H^+) - \Delta G^0_{(sol)}(AH)$

$\Delta G^0_{(g)}(AH) = 2.303\ RTpK_a(AH)$

$$\text{Direct } pK_a(AH) = \frac{\Delta G^0_{(g)}(AH)}{2.303\ RT}$$

Linear correction pK_a = (Direct pK_a + 7.281)/1.194

System	Molecular structure	HOMO	LUMO
COPT (gas phase)	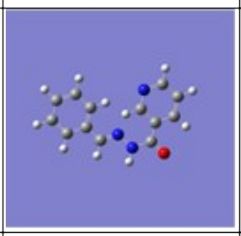	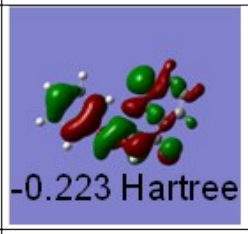 -0.223 Hartree	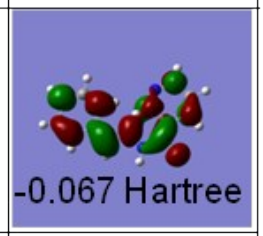 -0.067 Hartree
H_2S-COPT (gas phase)	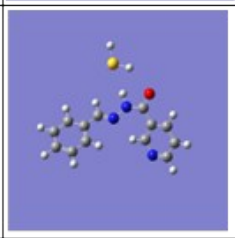	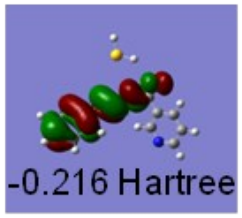 -0.216 Hartree	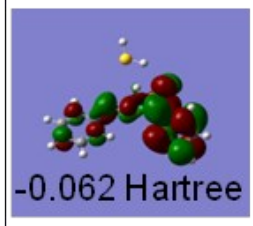 -0.062 Hartree
CO_2-COPT (gas phase)	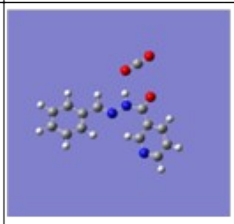	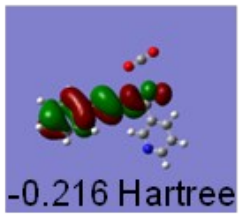 -0.216 Hartree	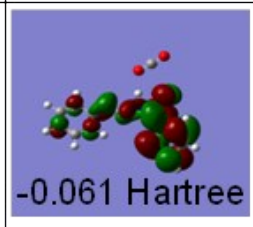 -0.061 Hartree
Deprotonated COPT (solution phase)	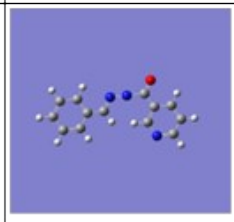	 -0.112 Hartree	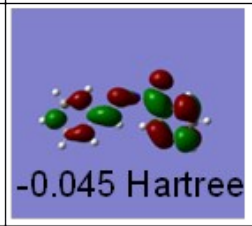 -0.045 Hartree
COPT (solution phase)	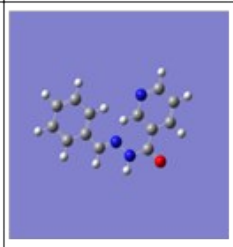	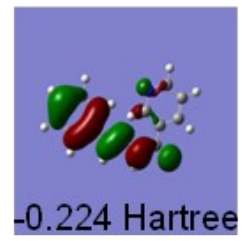 -0.224 Hartree	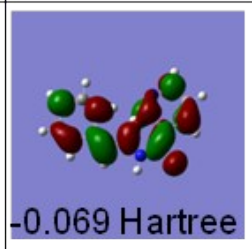 -0.069 Hartree
Deprotonated COPT (gas phase)	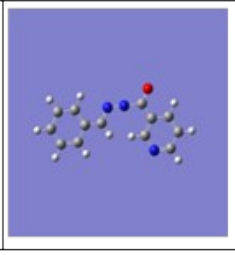	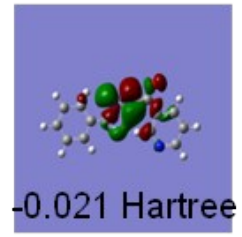 -0.021 Hartree	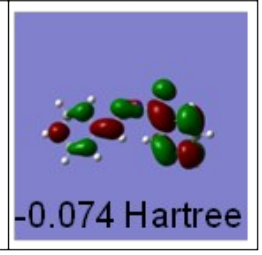 -0.074 Hartree

Summary of all DFT calculations (Basis set = 3-21G, Basis function = B3LYP, Solvation = The conductor-like polarizable continuum model CPCM/water)).

Now, if we include the effect of moisture, H_2S (week acid) generates HS^- and S^{2-} after reaction with moisture whereas CO_2 forms H_2CO_3 (week acid) upon reaction with moisture.

$$H_2S + H_2O = HS^- + H_3O^+$$

$$HS^- + H_2O = S^{2-} + H_3O^+$$

Now HS^- will more prone to interact with –HN-C(=O) rather than H_2CO_3. After exposure with H_2S, the proton transportation channel gradually collapses due to $H_2S\cdots$H-N-(C=O) interaction. In H_2S environment, the stability or percentage of enol form becomes lower due to $H_2S\cdots$H-N-(C=O) interaction. As a result, the electrical resistance of **COP** increases or suddenly changes in presence of H_2S and very fast response was observed for H_2S.

Supporting References

1) P. Gabbott, Principles and applications of thermal analysis. (Ed.), (2008), UK, John Wiley & Sons.
2) J. D. Menczel and R. B. Prime, Thermal analysis of polymers: fundamentals and applications. (Eds.). (2014), UK, John Wiley & Sons.
3) S. K. Das, P. Bhanja, S. K. Kundu, S. Mondal and A. Bhaumik, *ACS Appl. Mater. Interfaces* 2018, **10**, 28, 23813-23824.
4) V. Oklejas, R. H. Uibel, R. Horton and J. M. Harris, *Anal. Chem*. 2008, **80**, 1891-1901.
5) M. Mohan, M. N. Satyanarayan and D. R. Trivedi, *New J. Chem*. 2019, **43**, 10413-10428.
6) S. Mondal, S.; Y. Agam, R. Nandi and N. Amdursky, *Chem. Sci*. 2020, **11**, 3547-3556.
7) S. Rani, M. Kumar, R. Garg, S. Sharma and D. Kumar, *IEEE Sens. J*, 2016, **16** , 2929 - 2934.
8) M. K. Krepps, S. Parkin and D. A. Atwood, *Crystal Growth & Design* 2001, **1**, 291-297.
9) C. P. Kelly, C. J. Cramer and D. J. Truhla, *J. Phys. Chem. B* 2007, **111**, 408-422.